

Improving Dense Crowd Counting Convolutional Neural Networks using Inverse k -Nearest Neighbor Maps and Multiscale Upsampling

Greg Olmschenk¹

Hao Tang²

Zhigang Zhu^{1,3}

¹The Graduate Center of the City University of New York

²Borough of Manhattan Community College - CUNY

³The City College of New York - CUNY

golmschenk@gradcenter.cuny.edu, htang@bmcc.cuny.edu, zhu@cs.cuny.cuny.edu

Abstract

Gatherings of thousands to millions of people occur frequently for an enormous variety of events, and automated counting of these high density crowds is used for safety, management, and measuring significance of these events. In this work, we show that the regularly accepted labeling scheme of crowd density maps for training deep neural networks is less effective than our alternative inverse k -nearest neighbor ($ikNN$) maps, even when used directly in existing state-of-the-art network structures. We also provide a new network architecture MUD- $ikNN$, which uses multi-scale upsampling via transposed convolutions to take full advantage of the provided $ikNN$ labeling. This upsampling combined with the $ikNN$ maps further outperforms the existing state-of-the-art methods. The full label comparison emphasizes the importance of the labeling scheme, with the $ikNN$ labeling being particularly effective. We demonstrate the accuracy of our MUD- $ikNN$ network and the $ikNN$ labeling scheme on a variety of datasets.

1. Introduction

Every year, gatherings of thousands to millions occur for protests, festivals, pilgrimages, marathons, concerts, and sports events. For any of these events, there are countless reasons to desire to know how many people are present. For those hosting the event, both real-time management and future event planning is dependent on how many people are present, where they are located, and when they are present. For security purposes, knowing how quickly evacuations can be executed and where crowding might pose a threat to individuals is dependent on the size of the crowds. In journalism, crowd sizes are frequently used to measure the significance of an event, and systems which can accurately report on the event size are important for a rigorous evaluation.

Many systems have been proposed for crowd counting

purposes, with most recent state-of-the-art methods being based on convolutional neural networks (CNNs). To the best of our knowledge, nearly all modern CNN approaches which have been proposed rely on using a density map of individuals, primarily with a Gaussian based distribution of density values centered on individuals labeled in the ground truth images. Often, these density maps are generated with the Gaussian distribution kernel sizes being dependent on a k -Nearest Neighbor (kNN) distance to other individuals [18]. In this work, we explain how this generally accepted density map labeling is flawed and how an alternative inverse kNN ($ikNN$) labeling scheme, which does not explicitly represent crowd density, provides improved accuracy. We will show how a single $ikNN$ map provides information similar to an any arbitrary number of density maps with different Gaussian spreads, in a form which is better suited for neural network training. It provides a significant gradient spatially across the entire label and yet still provides precise location information of individual pedestrians (with the only exception being exactly overlapping head labelings). We show that by simply replacing density map training in an existing state-of-the-art network with our $ikNN$ map training, the testing accuracy of the network improves. This is the first major contribution of the paper.

Additionally, coupling multi-scale upsampling with densely connected convolutional networks [6] and our proposed $ikNN$ mapping, we provide a new network structure, MUD- $ikNN$, which outperforms the existing state-of-the-art methods, which uses multi-scale upsampling with transposed convolutions [16] to make effective use of the full ground truth label, particularly with respect to our $ikNN$ labeling scheme. The transposed convolutions are used to spatially upsample intermediate feature maps to the ground truth label map size for comparison. This approach provides several benefits. First, it allows the features of any layer to be used in the full map comparison, where many existing methods require a special network branch for this compari-

son. Notably, this upsampling, comparison, and following regression module can be used at any point in any CNN, with the only change being the parameters of the transposed convolution. This makes the module useful not only in our specific network structure, but it is also applicable in future state-of-the-art general purpose CNNs. Second, as this allows features which have passed through different levels of convolutions to be compared to the ground truth label map, this intrinsically provides a multi-scale comparison without any dedicated additional network branches, thus preventing redundant parameters which occur in separate branches. Third, because the transposed convolution can provide any amount of upsampling (again, with the features being used to specify the upsampling transformation), the upsampled size can be the full label ground truth size. In contrast, most existing works used a severely reduced size label map for comparison. These reduced sizes remove potentially useful training information. This proposed network structure is the second major contribution of the paper.

The paper is organized as follows. Section 2 discusses related work. Section 3 describes the proposed k -nearest neighbor map labeling method and its justification. Section 3 proposes our new network architecture for crowd counting, MUD- ik NN. Section 5 presents experimental results on several crowd datasets, and analyzes the findings. Finally, in Section 6 we provide a few concluding remarks.

2. Related Work

Many works use explicit detection of individuals to count pedestrians [15, 10, 14]. However, as the number of people in a single image increase and a scene becomes crowded, these explicit detection methods become limited by occlusion effects. Early works to solve this problem relied on global regression of the crowd count using low level features [2, 4, 3]. While many of these methods split the image into a grid to perform a global regression on each cell, they still largely ignored detailed spatial information of pedestrian locations. [9] introduced a method of counting objects using density map regression, and this technique was shown to be particularly effective for crowd counting by [17]. Since then, most works using deep neural networks for crowd counting have used density maps as a central role of their cost function [8, 12, 13, 17, 18].

A primary advantage of the density maps is the ability to provide a useful gradient for network training over large portions of the image spatially, which helps the network identify which portion of the image contains information signifying an increase in the count. These density maps are usually modeled by representing each labeled head position with a Dirac delta function, and convolving this function with a 2D Gaussian kernel [9]. This forms a density map where the sum of the total map is equal to the total count of individuals, while the density of a single individual is spread out over

several pixels of the map. The Gaussian convolution allows a smoother gradient for the loss function of the CNN to operate over, thereby allowing slightly misplaced densities to result in a lower loss than significantly misplaced densities.

In these works, the spread parameter of the Gaussian kernel is often determined using a k -nearest neighbor (k NN) distance to other head positions [18]. This provides a form of pseudo-perspective which results in pedestrians which are more distant from the camera (and therefore smaller in the image) having their density spread over a smaller number of density map pixels. While this mapping will often imperfectly map perspective (especially in sparsely crowded images), it works well in practice.

In a recent work[8], the authors used multiple scales of these k NN-based, Gaussian convolved density maps to provide various levels of spatial information, from large Gaussian kernels (allowing for a wide spread training gradient) to small Gaussian kernels (allowing for a precise localization of density). While this approach effectively integrates information from multiple Gaussian scales, thus providing both wide spread and precise training information, the network is left with redundant structures and how the various scales are chosen is fairly ad hoc. Our alternative ik NN labeling method supersedes these multiple scale density maps by providing both a smooth training gradient and precise localization in a single label. Our new network structure utilizes a single branch CNN structure for multi-scale regression. Together with the ik NN labeling it effectively provides the benefits of an arbitrary number of scales of these density maps.

3. Inverse k -nearest neighbor map labeling

We propose using full image size ik NN maps as an alternative labeling scheme from the commonly used density map explained in Section 2. Formally, the commonly used density map [8, 12, 13, 17, 18] is provided by,

$$D(\mathbf{x}, f(\cdot)) = \sum_{h=1}^H \frac{1}{\sqrt{2\pi}f(\sigma_h)} \exp\left(-\frac{(x-x_h)^2 + (y-y_h)^2}{2f(\sigma_h)^2}\right), \quad (1)$$

where H is the total number of head positions for the example image, σ_h is a size determined for each head position (x_h, y_h) using the k NN distance to other heads positions, and f is a manually determined function for scaling σ_h to provide a Gaussian kernel size. For simplicity, in our work we define f as a simple scalar function given by $f(\sigma_h) = \beta\sigma_h$, with β being a hand-picked scalar. Though they both apply to head positions, the use of k NN for σ_h in the density map is not to be confused with the full k NN map used in our

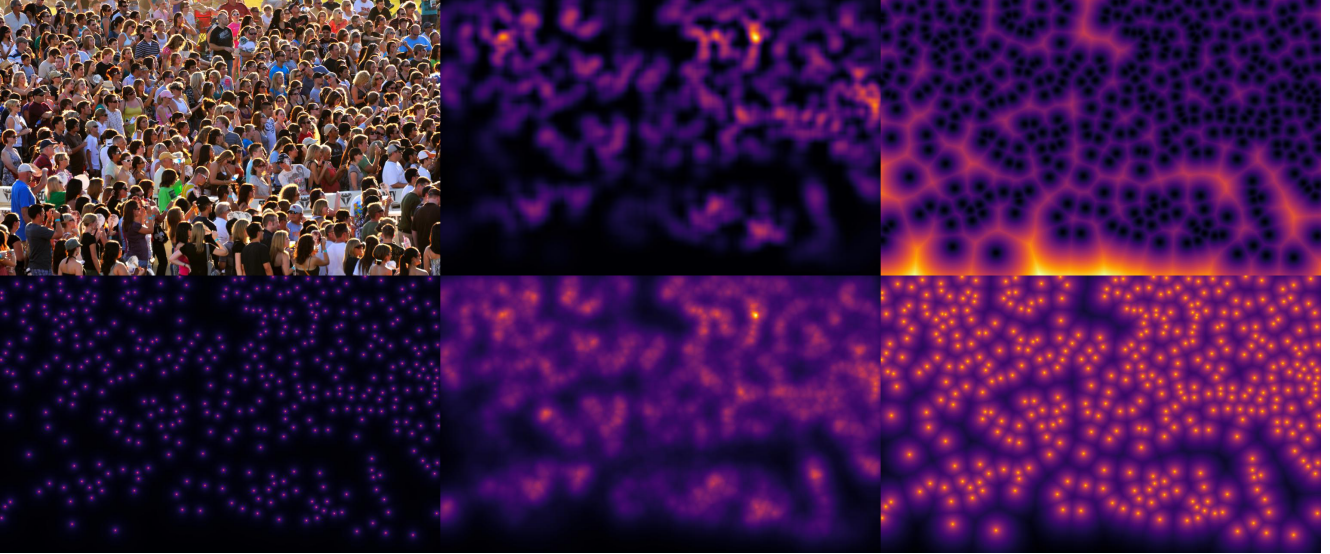


Figure 1: An example of a crowd image and various kinds of labelings. From left to right, top to bottom there is the original image, a density map, the k NN map with $k = 1$, the inverse k NN map with $k = 1$, the inverse k NN map with $k = 3$, and the inverse k NN map with $k = 1$ shown with a log scaling. Note, in the case of the density map, any values a significant distance from a head labeling are very small, and a log scaling shows a similar map as the non-log scaling. This is in contrast to the inverse k NN map, which has a significant gradient even a significant distance from a head position.

method, which is defined by,

$$K(x, k) = \frac{1}{k} \sum \min \left(\sqrt{(x - x_h)^2 + (y - y_h)^2}, \forall \mathbf{h} \in \mathcal{H} \right), \quad (2)$$

where \mathcal{H} is the list of all head positions. In other words, the k NN distance from each pixel, (x, y) , to each head position, (x_h, y_h) , is calculated. Additionally, we clip the maximum value of this k NN map to some variable, τ . We specified τ as half of the image patch size, as this is the maximum distance from any pixel to the edge of the input image patch. τ is chosen this way because the network is not expected to make a prediction of head locations beyond the scope of the input image patch.

After this, to produce the inverse k NN (ik NN) map, we use,

$$M = \frac{1}{K + 1}, \quad (3)$$

where M is the resulting ik NN map, with the addition and inverse being applied element-wise.

To understand the advantage of an ik NN map over a density map, we can consider taking the generation of density maps to extremes with regard to the spread parameter of the Gaussian kernel provided by f . A similar explanation is illustrated in Figure 2. At one extreme, is a Gaussian kernel with zero spread. Here the delta function remains unchanged, which in practical terms translates to a density map where the density for each pedestrian is fully residing on a single

pixel. When the difference between the true and predicted density maps is used to calculate a training loss, the network predicting density 1 pixel away from the correct labeling is considered just as incorrect as 10 pixels away from the correct labeling. Obviously, this is not desired, as it both creates a discontinuous training gradient, and the training process is intolerant to minor spatial labeling deviations. The other extreme is a very large Gaussian spread. This results in inexact spatial information of the location of the density. At the extreme, this provides no benefit over a global regression, which is the primary purpose for using a density map in the first place. Any intermediate Gaussian spread has an intermediate degree of both these problems. Using multiple scales of Gaussian spread, [8] tries to obtain the advantage of both sides. However, the size of the scales and the number of scales are then arbitrary and hard to determine.

In contrast, a single ik NN map as we have proposed provides all the required information from any arbitrary number of density maps with different Gaussian spreads. It provides a continuous spatial gradient everywhere and yet still provides the exact locations of individual pedestrians (with the only exception being exactly overlapping head labelings). An example of our ik NN map compared with a corresponding density map labeling can be seen in Figure 1.

Notably, [8] uses 3 density maps with different Gaussian spread parameters, with the Gaussian spread being determined by the k NN distance to other head positions multiplied by one of the 3 spread parameters. We note that for

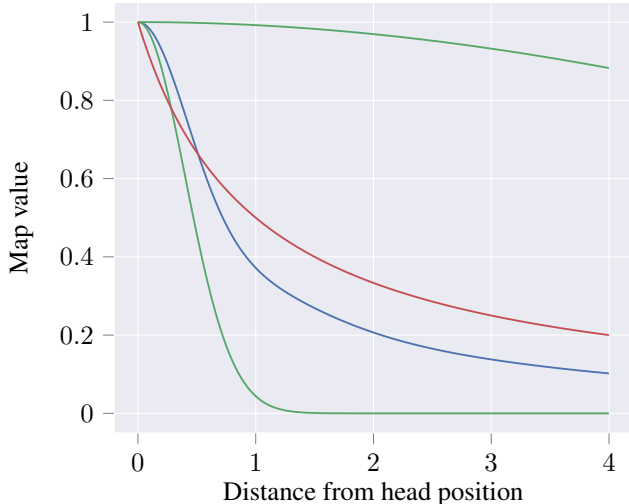


Figure 2: A comparison of the values of map labeling schemes with respect to the distance from an individual head position (normalized for comparison). Two Gaussians are shown in green. the narrow Gaussian provides a precise location of the head labeling, however, it provides little training information as the distance from the head increases. The wide Gaussian provides training information at a distance, but gives an imprecise location of the head position, resulting in low training information near the correct answer. The blue line shows a composite several Gaussians with spread parameters between those of the two extreme Gaussians ([8] uses 3 Gaussian spreads in their work). This provides both precise and distant training losses. Our approach of the i_k NN map shown in red (with $k = 1$) approaches a map function with a shape similar to the integral on the spread parameter of all Gaussians for a spread parameter range from 0 to some constant. Additionally, our method provides both the precise and distant training information in a single map label.

a single head position, all Gaussian distributions integrated over the spread parameter from 0 to some constant α results in a form of the incomplete gamma function. This function has a cusp around the center of the Gaussians. Similarly, the inverse of the k NN map also forms a cusp at the head position, and results in similar gradients of loss given misplaced density/distance values. In our experiments we found that an inverse k NN map outperformed density maps with ideally selected spread parameters.

As one experiment, we use [8]’s network architecture, which utilized DenseBlocks [6] as the basis, but we replace the density maps with i_k NN maps and show there is an improvement in the prediction’s mean absolute error. This demonstrates the direct improvement of our i_k NN method on an existing state-of-the-art network. Note, the regression module from i_k NN map to count is then also required to

convert from the i_k NN map to a count. The difference in error between the original approach in [8] and the network in [8] with our i_k NN maps, though improved, is relatively small. We suspect this is because the density maps (or i_k NN maps) used during training are downsampled to a size of 28×28 (where the original images and corresponding labels are 224×224). This severe downsampling results in more binning of pixel information, and this seems to reduce the importance of which system is used to generate that label. At the extreme case, when downsampled to a single value, both approaches would only give an the global count in the patch (where the i_k NN map gives the inverse of the average distance from a pixel to a head labeling which can be translated to an approximate count). This downsampling is a consequence of the network structure only permitting labels of the same spatial size as the output of the DenseBlocks. Our network (which will be described below) remedies this through transposed convolutions, allowing for the use of the full size labels.

4. MUD- i_k NN: a new network architecture

We propose a new network structure with both multi-scale upsampling using DenseBlocks [6] and our i_k NN mapping scheme (thus MUD- i_k NN). We show that the new MUD- i_k NN structure out-performs the existing state-of-the-art networks. In addition to the use of i_k NN maps playing a central role, we also demonstrate how features with any spatial size can contribute in the prediction of i_k NN maps and counts through the use of transposed convolutions. This allows features of various scales from throughout the network to be used for the prediction of the crowd.

The proposed MUD- i_k NN network structure is shown in Figure 3. Our network uses the DenseBlock structures from DenseNet201 [6] in their entirety. DenseNet has been shown to be widely applicable to various problems. From their structure, we make the several important modifications. The output of each DenseBlock (plus transition layer) is used as the input to the following DenseBlock, just as it is in DenseNet201. However, each of these outputs are also passed to a transposed convolutional layer (excluding the final DenseBlock output). These transposed convolutions are given a stride and kernel size such that output is the size of the i_k NN map, and no spatial input dimensions have their output overlap in the produced i_k NN map. This form of upsampling allows the feature depth dimensions to contribute to the gradients of the map values in the predicted i_k NN map. Both the stride and kernel size of the transposed convolutions of our network are 8, 16, and 32.

The i_k NN map generated at each level is individually compared against the ground truth i_k NN map, each produc-

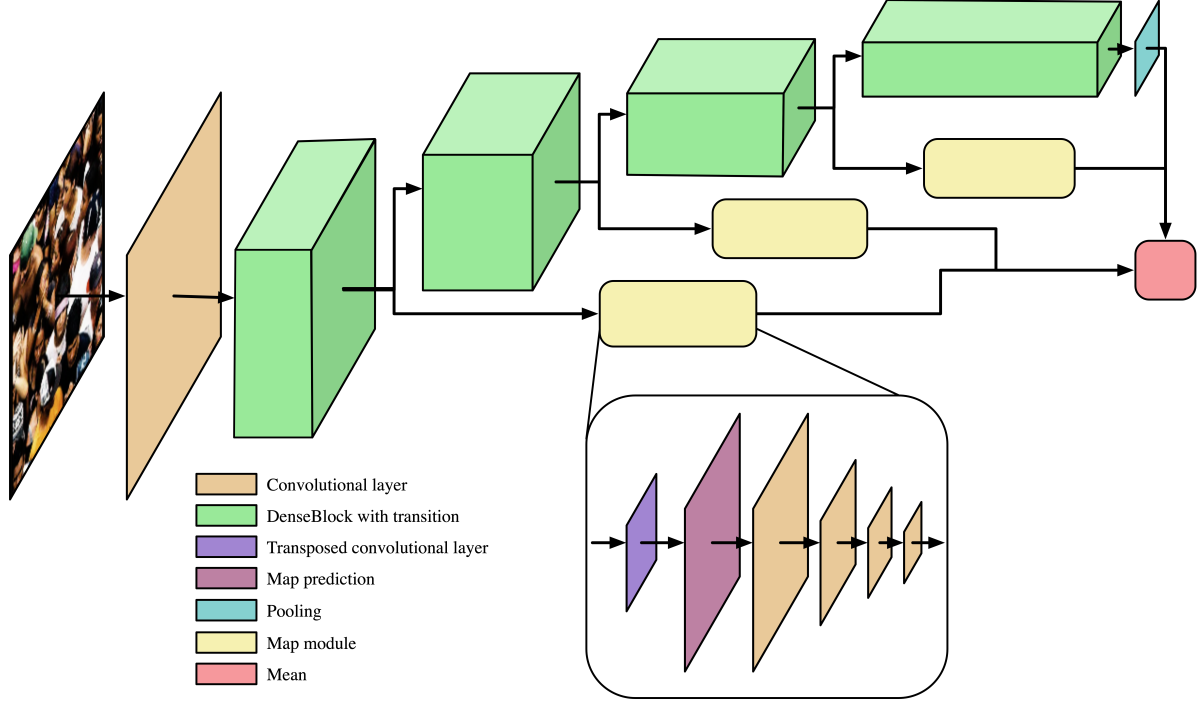


Figure 3: A diagram of the proposed network architecture MUD- ik NN: multiscale regression with DenseBlocks and ik NN mapping. (Best viewed in color)

ing a loss which is then summed,

$$\mathcal{L}_m = \sum_j \text{MSE}(\hat{M}_j, M_j) \quad (4)$$

where j is the index of the DenseBlock that the output came from, M is the ik NN map labeling, and \hat{M} is the predicted map labeling.

Each ik NN map is then also used as the input to a small regression module. This module is a series of small convolutional layers, shown in the inset of Figure 3. The sizes of these layers are specified in Table 1. The regression module then has a singleton output, corresponding to the predicted crowd count.

The mean of all predicted crowd counts from the regression modules, three in Figure 3, and the output of the final DenseBlock is used as the final count prediction.

$$\mathcal{L}_c = \text{MSE} \left(\frac{\hat{C}_{end} + \sum_{j=1}^m \hat{C}_j}{m+1}, C \right) \quad (5)$$

with C being the ground truth count, \hat{C}_{end} being the regression count output by the final DenseBlock, and \hat{C}_j being the count from the j th map regression module ($j = 1, 2, \dots, m; m = 3$ in Figure 3). This results in a total loss given by $\mathcal{L} = \mathcal{L}_m + \mathcal{L}_c$.

Layer	Output size	Filter
Input from DenseBlock	128x28x28 256x14x14 896x7x7	
Transposed convolution	1x224x224 (map prediction)	(8,16,32)x(8,16,32) stride=(8,16,32)
Convolution	8x112x112	2x2 stride=2
Convolution	16x56x56	2x2 stride=2
Convolution	32x28x28	2x2 stride=2
Convolution	1x1x1	28x28

Table 1: A specification of the map module layers. This module is used at 3 points throughout our network as shown in Figure 3, so the initial input size varies. However, the transposed convolution always produces a predicted map label which is uniform size (1x224x224).

This approach has multiple benefits. First, if an appropriately sized stride and kernel size is specified, the transposed convolutional layer followed by ik NN map prediction to regression module can accept any sized input. This means this module of the network is very generalizable and can be applied to any CNN structure at any point in the network.

For example, an additional DenseBlock could be added to either end of the DenseNet, and another of these map modules could be attached. Second, each i k NN map is individually trained to improve the prediction at that layer, which provides a form of intermediate supervision, easing the process of training earlier layers in the network. At the same time, the final count is based on the mean values of the regression modules. This means that if any individual regression module produces more accurate results, its results can individually be weighted as being more important to the final prediction.

We note that the multiple Gaussian approach by [8] has some drawbacks. The spread of the Gaussians as well as the number of different density maps is somewhat arbitrary. Perhaps more importantly, where each Gaussian map is generated and compared is slightly counter-intuitive. Their final Gaussian map with a spread of zero is generated and compared after the most convolutions have occurred. Intuitively, we would expect the most precise location information to come after the least number of convolutions, as the receptive field in the original image is still small and precise. Once again, our network avoids complications here by providing both precise labelings and wide spread labelings in every i k NN map.

The input to the network is 224x224 image patches. The i k NN maps (or density maps) use the same size patches (contrary to most methods which use a downsampled label). Each map regression module contains the layers specified in Table 1. At evaluation time, a sliding window with a step size of 128 was used for each patch of the test images, with overlapping predictions were averaged.

Network code, hyperparameters, and trained models can be found at <https://github.com/golmschenk/sr-gan>.

5. Results

5.1. Evaluation metric

For each dataset that we evaluated our method on, we provide the mean absolute error (MAE), normalized absolute error (NAE), and root mean squared error (RMSE). These are given by the following equations:

$$\text{MAE} = \frac{1}{N} \sum_{i=1}^N |\hat{C}_i - C_i| \quad (6)$$

$$\text{NAE} = \frac{1}{N} \sum_{i=1}^N \frac{|\hat{C}_i - C_i|}{C_i} \quad (7)$$

$$\text{RMSE} = \sqrt{\frac{1}{N} \sum_{i=1}^N (\hat{C}_i - C_i)^2} \quad (8)$$

Method	MAE	NAE	RMSE
Idrees <i>et al.</i> (2013) [7]	315	0.63	508
MCNN [18]	277	0.55	426
Encoder-Decoder [1]	270	0.56	478
CMTL [13]	252	0.54	514
SwitchCNN [12]	228	0.44	445
Resnet101 [5]	190	0.50	227
DenseNet201 [6]	163	0.40	226
Idrees <i>et al.</i> (2018) [8]	132	0.26	191
[8] with i1NN maps	122	0.252	195
MUD-i1NN	104	0.209	172

Table 2: Results on the UCF-QNRF dataset compared with various existing works.

We attempt to give as many relevant comparisons to the state-of-the-art as possible. Most works provide their MAE and RMSE results. [8] provided the additional metric of NAE. Though this result is not available for many of the datasets, we provide our own NAE on these datasets for future works to refer to. Though [8] is one of the most accurate state-of-the-art results compared to in this work, they have only provided their results for their latest dataset UCF-QNRF. As such, their results only appear in regard to that dataset.

Unless otherwise noted, $k = 1$ was used for the i k NN map labels (thus i1NN map labels).

5.2. UCF-QNRF dataset

The first dataset we evaluated our approach on is the UCF-QNRF dataset [8], which contains 1535 total images split as 1201 training images and 334 testing images. These training and testing distributions are provided by the dataset provider. The dataset contains 1,251,642 total head count, with a median of 425 (per image), a mean of 815.4, a minimum of 49, and a maximum of 12,865. The results of our MUD- i k NN network compared with other state-of-the-art networks can be seen in Table 2. Our network significantly out-performs the existing methods.

Along with a comparison of our complete method compared with the state-of-the-art, we compare with [8]’s network, but replacing their density map predictions and summing to count with our i k NN map prediction and regression to count. Using the i k NN maps, we see that their model sees improvement in MAE with i k NN maps, showing the effect of the i k NN mapping. Nevertheless, i k NN mapping with our new network architecture (MUD- i k NN) significantly overperforms the i k NN mapping with the network in [8], indicating the effectiveness of our new network architecture.

Method	MAE	NAE	RMSE
Zhang <i>et al.</i> [17]	181.8	-	277.7
MCNN [18]	110.2	-	173.2
SwitchCNN [12]	90.4	-	135.0
MUD-i1NN 28x28	75.8	0.180	120.3
MUD-i1NN	70.4	0.169	112.7
MUD-i2NN	67.9	0.162	109.5
MUD-i3NN	67.7	0.162	108.9

Table 3: Results on the ShanghaiTech Part A dataset compared with various existing works.

Method	MAE	NAE	RMSE
Zhang <i>et al.</i> [17]	32.0	-	49.8
MCNN [18]	26.4	-	41.3
SwitchCNN [12]	21.6	-	33.4
MUD-i1NN	14.4	0.124	20.0

Table 4: Results on the ShanghaiTech Part B dataset compared with various existing works.

5.3. ShanghaiTech dataset

The second dataset we evaluated our approach on is the ShanghaiTech dataset [18]. This dataset contains a total of 330,165 head position labelings. The dataset is split into two parts, Part A and Part B. For both parts, we used the training and testing images as prescribed by the dataset provider.

Part A contains 482 images, 300 for training and 182 for testing. It contains a total of 241,677 head labelings, with an average of 501.4, a maximum of 3139, and a minimum of 33. The results of our evaluation on this dataset can be seen in Table 3. Once again, our MUD- i kNN network significantly outperforms the state-of-the-art approaches on this dataset.

Part B contains 716 images, 400 for training and 316 for testing. It contains a total of 88,488 head labelings, with an average of 123.6, a maximum of 578, and a minimum of 9. The results of our evaluation on this dataset can be seen in Table 4. Consistent performance is achieved on this dataset.

Our network and i kNN labeling method significantly outperforms the state-of-the-art methods.

5.4. UCF-CC-50 dataset

The third dataset we evaluated our approach on is the UCF-CC-50 dataset [7]. This dataset contains a total of 63,705 head position labelings over 50 images. The head labelings in its images have an average of 1280, a maximum of 4543, and a minimum of 94. We followed the standard evaluation metric for this dataset of a five-fold cross evaluation. The results of our evaluation on this dataset can be seen in Table 5.

Method	MAE	NAE	RMSE
Zhang <i>et al.</i> [17]	467.0	-	498.5
MCNN [18]	377.6	-	509.1
Hydra2s[11]	333.73	-	425.26
SwitchCNN [12]	318.1	-	439.2
MUD-i1NN	237.76	0.191	305.68

Table 5: Results on the UCF-CC-50 dataset compared with various existing works.

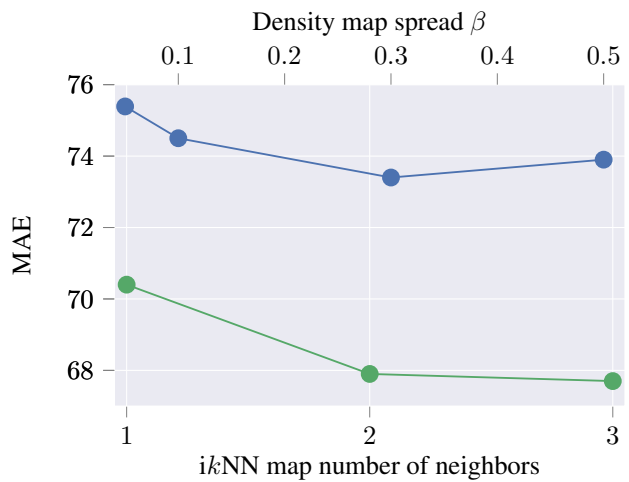


Figure 4: A comparison of the errors from training with density maps using various spread parameters ($\beta = 0.05, 0.1, 0.3, 0.5$, in blue), and i kNN maps using various numbers of neighbors ($k = 1, 2, 3$, in green). These experiments were performed on the ShanghaiTech dataset part A.

5.5. Density maps vs i kNN maps

We trained our network using various density maps produced with different Gaussian spread parameters, β (as described in Section 3), and compared these results to the network using i kNN maps with varying k . These tests were performed on the ShanghaiTech dataset part A. The results of these tests can be seen in Figure 4. Here we see that (1) the i kNN maps (with all k values we tested $k = 1, 2, 3$) can outperform the best spread parameter for the density map (where $\beta = 0.3$); (2) for this dataset, the performance improves with increasing k . The tests from $k = 1$ to $k = 3$ suggests that an increasing k provides benefits, but with a diminishing return. While this intuitively seems reasonable, the experiments were limited to only 3 values of k on a single dataset, so this conclusion is speculative.



(a) i1NN predictions.

(b) i3NN predictions.

Figure 5: A small sample of patch predictions for map labels. In each subfigure, from left to right is the original image patch, the ground truth label, and the patches from the three map modules in order through the network.

5.6. Upscaling Analysis

Nearly all existing works using a density map use a reduced size label for testing. This may be because it requires less network parameters, but it usually seems to be a consequence of network structure. Again, our map module avoids this constraint by upsampling the label using a trained transposed convolution. Using the ShanghaiTech part A dataset, we tested our network using the full 224x224 size i1NN maps compared with ones which were resized to 28x28 (matching the label sizes used in [8]) to test how much of an impact the label resolution has on the predictive abilities of the network. These results can be seen in Table 3. Note, a small modification had to be made to the convolutions leading to the regression in the map module to accommodate the small label size. Specifically, the first convolution as remove (as 28 is only divisible by 2 twice), and then the final convolution kernel size was reduced to 7. A set of predicted i_k NN map labels can be seen in Figure 5. The reader may notice a grid pattern appearing in these predicted labels (particularly noticeable in Figure 5b). Each portion of the predicted map comes from a 1x1 set of features and is upsampled by 8, 16, and 32 pixels for the respective map modules in the network. Hence, the tiles of the grid have dimensions of 8, 16, and 32 in the predicted maps. Note, the inter-tile pixels are not a uniform value. More examples of map predictions can be found in the supplementary material.

5.7. General Analysis

For each dataset we evaluated, our i_k NN method combined with our new network architecture (MUD- i_k NN) significantly outperforms the existing state-of-the-art approaches. Additionally, our i_k NN method produced improved results using [8]’s network structure. This shows the improvements to be gained by simply replacing the density map labeling with our i_k NN map labeling.

Although our new approach outperformed the existing methods in all cases, the improvement appears to be more significant on larger databases. For the UCF-QNRF database containing $>1M$ head labelings, our approach resulted in less than half (48%) the MAE as SwitchCNN [12]. However, on the much smaller dataset of ShanghaiTech Part B, which contains $<100K$ head labelings, our approach results in 73% the error of SwitchCNN. This is likely due to the size of the network relative to the amount of data available. Another possibility is that the UCF-QNRF dataset contains a more diverse set of scenes, and our approach may handle this diversity better.

6. Conclusions

In this work, we have presented a new form of labeling for crowd counting data, the i_k NN map. We have compared this labeling scheme to commonly accepted labeling approach for crowd counting, the density map. We show that using the i_k NN map with an existing state-of-the-art network improves the accuracy of the network compared to density map labelings. Additionally, we presented a new network structure, MUD- i_k NN, which is generalizable and takes full advantage of our i_k NN map labeling. We show on various datasets that our network architecture significantly outperforms the existing state-of-the-art networks.

This work presents several opportunities for future investigation. First, the use of both i_k NN maps and the map module in other network structures can be explored. Next, a deeper evaluation of the influence of various values of k may provide interesting insights. Finally, this work only provides one possible improvement over a density map labeling. There may be a more effective variant labeling yet to be discovered.

References

- [1] V. Badrinarayanan, A. Kendall, and R. C. SegNet. A deep convolutional encoder-decoder architecture for image segmentation. *arXiv preprint arXiv:1511.00561*. 6
- [2] A. B. Chan, Z.-S. J. Liang, and N. Vasconcelos. Privacy preserving crowd monitoring: Counting people without people models or tracking. In *Computer Vision and Pattern Recognition, 2008. CVPR 2008. IEEE Conference on*, pages 1–7. IEEE, 2008. 2
- [3] K. Chen, S. Gong, T. Xiang, and C. Change Loy. Cumulative attribute space for age and crowd density estimation. In *Proceedings of the IEEE conference on computer vision and pattern recognition*, pages 2467–2474, 2013. 2
- [4] K. Chen, C. C. Loy, S. Gong, and T. Xiang. Feature mining for localised crowd counting. In *BMVC*, volume 1, page 3, 2012. 2
- [5] K. He, X. Zhang, S. Ren, and J. Sun. Deep residual learning for image recognition. In *Proceedings of the IEEE conference on computer vision and pattern recognition*, pages 770–778, 2016. 6
- [6] G. Huang, Z. Liu, L. Van Der Maaten, and K. Q. Weinberger. Densely connected convolutional networks. In *CVPR*, volume 1, page 3, 2017. 1, 4, 6
- [7] H. Idrees, I. Saleemi, C. Seibert, and M. Shah. Multi-source multi-scale counting in extremely dense crowd images. In *Proceedings of the IEEE conference on computer vision and pattern recognition*, pages 2547–2554, 2013. 6, 7
- [8] H. Idrees, M. Tayyab, K. Athrey, D. Zhang, S. Al-Maadeed, N. Rajpoot, and M. Shah. Composition loss for counting, density map estimation and localization in dense crowds. *arXiv preprint arXiv:1808.01050*, 2018. 2, 3, 4, 6, 8
- [9] V. Lempitsky and A. Zisserman. Learning to count objects in images. In *Advances in neural information processing systems*, pages 1324–1332, 2010. 2
- [10] Z. Lin and L. S. Davis. Shape-based human detection and segmentation via hierarchical part-template matching. *IEEE Transactions on Pattern Analysis and Machine Intelligence*, 32(4):604–618, 2010. 2
- [11] D. Onoro-Rubio and R. J. López-Sastre. Towards perspective-free object counting with deep learning. In *European Conference on Computer Vision*, pages 615–629. Springer, 2016. 7
- [12] D. B. Sam, S. Surya, and R. V. Babu. Switching convolutional neural network for crowd counting. In *Proceedings of the IEEE Conference on Computer Vision and Pattern Recognition*, volume 1, page 6, 2017. 2, 6, 7, 8
- [13] V. A. Sindagi and V. M. Patel. Cnn-based cascaded multi-task learning of high-level prior and density estimation for crowd counting. In *Advanced Video and Signal Based Surveillance (AVSS), 2017 14th IEEE International Conference on*, pages 1–6. IEEE, 2017. 2, 6
- [14] M. Wang and X. Wang. Automatic adaptation of a generic pedestrian detector to a specific traffic scene. In *Computer Vision and Pattern Recognition (CVPR), 2011 IEEE Conference on*, pages 3401–3408. IEEE, 2011. 2
- [15] B. Wu and R. Nevatia. Detection of multiple, partially occluded humans in a single image by bayesian combination of edgelet part detectors. In *null*, pages 90–97. IEEE, 2005. 2
- [16] M. D. Zeiler, D. Krishnan, G. W. Taylor, and R. Fergus. Deconvolutional networks. 2010. 1
- [17] C. Zhang, H. Li, X. Wang, and X. Yang. Cross-scene crowd counting via deep convolutional neural networks. In *Proceedings of the IEEE Conference on Computer Vision and Pattern Recognition*, pages 833–841, 2015. 2, 7
- [18] Y. Zhang, D. Zhou, S. Chen, S. Gao, and Y. Ma. Single-image crowd counting via multi-column convolutional neural network. In *Proceedings of the IEEE conference on computer vision and pattern recognition*, pages 589–597, 2016. 1, 2, 6, 7